

Characterization of Microstructured Multiwalled Carbon Nanotube/Polydimethylsiloxane Composites for Piezoresistive Sensing Applications

Claudia S. Buga, Carlos J. Tavares, and Júlio C. Viana*

Technological advancements in the field of flexible and printed electronics are creating a need for large-area sensors that can be embedded over different types of surfaces. Such sensors can be used to monitor physical signals over flexible, curved, or soft devices. Hence, it is herein proposed, a formulation to produce piezoresistive multiwalled carbon nanotube/polydimethylsiloxane (MWCNT/PDMS) composites with tunable electric properties for pressure sensing purposes. The composite is obtained through few manufacturing steps, avoiding the use of hazardous solvents. Different weight percentages of MWCNT dispersed in PDMS are evaluated and the results evidence that using 3.0 wt% of infill is sufficient to obtain highly sensitive sensors. To enhance the dispersion of the MWCNT and add microstructure to the composite, a system composed of a surfactant and foaming agent is used. Finally, pressure sensing units and arrays are printed and tested. The sensors present fast response, low hysteresis, repeatability, and a sensing range of 0–160 kPa. The composite is more sensitive to lower pressure and a maximum sensitivity of 8.0% kPa⁻¹ is achieved for porous composites at pressure <10 kPa. Thanks to these characteristics, the sensors are successfully used in the development of a pressure sensing array and heartbeat sensor for proof of concept.

1. Introduction

As the interest in flexible, lightweight, and sustainable electronics is growing, there is the demand for innovative materials and reproducible manufacturing solutions for sensor development. Currently, silicon is still the most widely used semiconductive material in electronics. However, to address issues related to its processing, sustainability, and lack of flexibility, new materials are being developed.^[1] As a result, alternatives based on carbon allotropes, carbon-based composites, and electrically conductive polymers have become increasingly popular.^[2,3] Simultaneously, sensing-related technologies are developing rapidly, much as a response to the emergence of the Internet of Things (IoT).^[4] The fields of biomonitoring and electronic skins, which are used to monitor biofunctions and mimic the assets of the human skin, respectively, are prone to benefit extensively from the advancements arising in sensing technology.^[3,5–9]


Pressure sensing is one of the most important features to be used in these monitoring applications; nonetheless, their performance is still limited in terms of sensitivity, sensing range, response and recovery times, hysteresis, size, and lack of flexibility. As a result, researchers are focused on developing pressure sensors, with optimized designs, capable of granting the best possible compromise among the previously mentioned performance indicators.^[10,11] Moreover, to properly mimic human pressure sensing, sensors must present sensitivity in the range of at least 1–100 kPa, they should be able to distinguish between static and dynamic stimuli, have a fast response time, and present a linear response or, at least, defined linearity sensing zones.^[3,5–9] The sensitivity of the sensors reported in the literature varies vastly and can be adjusted using adequate data processing, notwithstanding, a high native sensitivity (0.5–34 kPa%) is yearned for, as summarized in Table S1, Supporting Information.^[12,13]

Pressure sensors can be capacitive, piezoelectric, or resistive.^[14] Capacitive and piezoelectric sensors are known to exhibit fast response, accuracy, and low hysteresis but are more suitable to read dynamic pressure signals, and the necessary electronic processing to acquire data is often complex. In contrast, piezoresistive sensors are a great alternative to read static and dynamic actuating pressure where an ultrafast response is not

C. S. Buga, J. C. Viana
IPC/LASI – Institute for Polymers and Composites/Associated Laboratory of Intelligence Systems
University of Minho
Campus de Azurém, 4800-058 Guimarães, Portugal
E-mail: jcv@dep.uminho.pt

C. S. Buga, J. C. Viana
DTx Colab – Digital Transformation
University of Minho
Campus de Azurém, 4800-058 Guimarães, Portugal

C. J. Tavares
CFUM – Centro de Física da Universidade do Minho
Campus de Azurém, 4800-058 Guimarães, Portugal

 The ORCID identification number(s) for the author(s) of this article can be found under <https://doi.org/10.1002/adem.202400132>.

© 2024 The Authors. Advanced Engineering Materials published by Wiley-VCH GmbH. This is an open access article under the terms of the Creative Commons Attribution-NonCommercial-NoDerivs License, which permits use and distribution in any medium, provided the original work is properly cited, the use is non-commercial and no modifications or adaptations are made.

DOI: 10.1002/adem.202400132

demanding, and simple interface electronics are required.^[14,15] To condition these circuits, basic voltage dividers or inverting amplifiers can be used and the data from each sensor can be read individually. When developing pressure sensors aimed at biomonitoring, human-machine interfacing, and e-skins, it is important to use soft, stretchable, and thin materials that can be attached to the surface of the skin or other curved, smooth, or deformable surfaces.^[6,16,17] Thus, these pressure sensors are usually produced resorting to composite materials encompassing a flexible polymer matrix filled with conductive carbon allotropes such as carbon nanofibers,^[18] carbon nanotubes (CNTs),^[19] graphene,^[20] carbon black (CB),^[21–23] or with conductive metallic materials including silver nanoparticles.^[24] Multiwalled CNTs (MWCNTs)/polydimethylsiloxane (PDMS) is one of the most used pressure sensing composites, as these affordable materials are frequently processed together and assure relatively high and stable electrical performance.^[17,25–27] However, to homogeneously disperse the MWCNT, researchers often resort to aggressive polar solvents such as toluene, methanol, and dimethylformamide because they grant a faster and longer-lasting dispersion of the nanotubes.^[28] In an effort to contradict this tendency, Rajendram et al. conducted a study using different solvents, namely water, ethanol, 2-propanol (IPA), and toluene to analyze their influence on the dispersion of MWCNT.^[28] According to their findings, the affinity of functionalized MWCNT is higher for water, followed by ethanol, IPA, and finally, toluene. Hence, good dispersion of the MWCNT should be achieved by using innocuous high-polar solvents such as water, ethanol, and isopropyl alcohol (IPA).

Adding microstructure within the sensing material has also been proven as an effective strategy to enhance the compressibility of materials, increasing their sensitivity, sensing range, and response time.^[6,10,13,23,24,29,30] Popular approaches include 1) the use of sacrificial materials such as sugar, salt, polycaprolactone, polystyrene, citric acid, and nickel;^[12,21,23,31–33] 2) foaming;^[34–37] 3) surface coating of template sponges;^[6,19,24,31] 4) melt-phase separation methods;^[29] 5) freeze drying;^[38] 6) mold structuring followed by mold casting;^[39–41] and 7) 3D printing.^[42] As an example, Carneiro and co-workers developed pressure sensors and a wearable pressure mapping device using CB-filled polyurethane foam. The foam was obtained by mixing fine sugar as template material and casting the composite in the desired shape. The sugar was later removed through sonication-aided dissolving.^[12] Using this methodology and optimizing the CB mass content to 14.43%, they were able to obtain multifunctional pressure sensors with high sensitivity (18 kPa^{-1}) for pressure lower than 5 kPa. However, the sensitivity decreased to only $0.1\% \text{ kPa}^{-1}$ for pressures from 5 to 100 kPa. The foam, which was about 4.5 mm thick, presented a response of 200 ms and showed low measurement hysteresis for over 15 000 cycles. Recently, Xia et al. focused on the development of linear and low hysteresis strain sensors, aimed at wearable electronic skins.^[23] To produce their sensors, they opted to develop a CB/PDMS sponge combining sacrificial templating with mold casting by pouring PDMS over a polytetrafluoroethylene mold, which had been previously stacked with NaCl particles. Their solution rendered their sensors fast response (100 ms), outstanding linearity, and high sensitivity ($8.3\% \text{ kPa}^{-1}$) until a strain of 76%. In another study, Ma and colleagues developed microstructured resistive pressure by mold

casting CNT/PDMS composites with 2 wt% CNT loading.^[13] The optimized sensor microstructure was pyramidal with a spacing of $12\ \mu\text{m}$ between micropyramids, which had a base length of $12\ \mu\text{m}$ each. This design allowed the researchers to develop sensors capable of transducing low-pressure ($<10\ \text{kPa}$) and medium-pressure ($10\text{--}100\ \text{kPa}$) regimes with a sensitivity of $34\% \text{ kPa}^{-1}$ and a response time of $\approx 48\ \text{ms}$.

Another alternative is to use chemical foaming agents to induce porosity. This can be achieved using carbonates, bicarbonates, nitrates, isocyanate, dichloromethane, dichloroethane, or physical foaming agents, such as nitrogen, xylene, carbon dioxide, air, or water.^[34,35] Li and co-workers used a one-step green foaming process to develop graphene oxide (GO)-coated porous silicone rubber foams (SiRFs).^[37] For this, they used dihydroxy PDMS (PDMS-OH) and mixed it with hydrogen dimethicone, GO, vinyl dimethicone, and Karstedt catalyst. The mixture was foamed at room temperature for 10 min and then cured in an air-dry oven for 2 h at $100\ ^\circ\text{C}$, which allowed them to obtain the porous SiRF-GO. Masihi and colleagues also developed a porous PDMS structure, which was used as a capacitive sensor. In their approach, they mixed the PDMS precursor with sodium bicarbonate (SB, NaHCO_3) in a 5:1 (w/w) ratio.^[43,44]

Drawing inspiration from the previous examples, this work intends to explore alternative and scalable manufacturing pathways to develop eco-friendly, and affordable pressure sensors that could be applied for the development of biomonitoring and electronic skin devices. Hence, the main goals are the production of thin, flexible, and sensitive pressure sensors as well as the investigation of the impact that microstructure has on the performance of the sensors, particularly in their working range and sensitivity. To achieve this, a new process to produce bulk and porous MWCNT/PDMS composites is proposed. Taking into account that the vast majority of porous sensors present in the literature are produced using (often bulky) sponges, achieved through sacrificial templating, mold casting, and dip coating of commercial sponges, it was decided to explore the phenomena of foaming instead. Thus, porosity was added resorting to a foaming approach based on the use of SB, as the foaming agent, and Triton X-100 for stabilization of the mixture. IPA, which is safe and inexpensive, was chosen as the solvent used for the dispersion of the MWCNT. Different infill percentages were tested and, considering the percolation threshold of the composite, a more extensive study was performed for 2.0, 3.0, and 5.5 wt% in MWCNT. The composites were then studied regarding their morphology, mechanical behavior, chemical composition, and electromechanical behavior. Finally, their applicability to the development of resistive pressure mapping arrays and heartbeat monitoring was evaluated.

2. Experimental Section

2.1. Materials

MWCNT NC7000, obtained from Nanocyl, was used as the functional fillers of the piezoresistive composite. PDMS Sylgard 184, obtained from DOWSIL, was used as the elastomeric matrix. IPA was selected as the solvent. The surfactant Triton X-100 was obtained from Sigma Aldrich. Off-the-shelf SB(NaHCO_3)

powder was used as the foaming agent. The silver electrodes and case study array were screen printed using a conductive silver paste from Dycotec, DM-SIP-30 655, over a substrate of piezoresistive MWCNT/PDMS composites are developed using a simple methodology. Different infill percentages of bulk and porous materials are produced and comparatively studied in terms of morphology, mechanical, and electromechanical characteristics. Porous composites with infill of 3.0 wt% are found to be more sensitive in the pressure range of interest. Further studies focusing on response and recovery times, repeatability, and usability in a 3×4 sensing array are pursued for porous 3.0 wt% MWCNT/PDMS composite PET from S. K. Chemicals, with a thickness of 75 μm . Polyimide tape, conductive copper tape, conductive wire connectors, Arduino boards, resistors, and breadboards were used to implement the applications and acquire data.

2.2. Methods

2.2.1. Production of the Piezoresistive Composites

First, the silver interdigitated electrodes were screen printed over polyethylene terephthalate (PET) using a manual Miniprint screen printer equipped with vacuum, purchased from Acosgraf. Two sets of MWCNT/PDMS composites were produced: one without microstructure (bulk) and another with microstructure (porous). This allowed to compare the electro-mechanical characteristics of the composites. To determine the percolation threshold of the piezoresistive bulk composite, the MWCNT was weighted in different MWCNT/PDMS percentages (0.1, 0.3, 0.5, 1.0, 2.0, 3.0, 5.5, 8.0, and 10.0 wt%). They were then dispersed in a system of Triton X-100, previously dissolved in 30 mL of IPA, using magnetic stirring, for 30 min

(Figure 1(1)). To grant a homogeneous dispersion of the MWCNT in the system, a Hielscher UP200Ht ultrasonic probe was used with 60% amplitude and 70 W of applied power, on intermittent pulses of 1 s for 30 min, as depicted in Figure 1(2). During this step, the temperature was controlled using an ice bath. To produce the microstructured composites, 10 wt% SB was added after this step, and an extra 10 min of ultrasonication was performed, under the same conditions. The PDMS prepolymer was dissolved in 20 mL of IPA resorting to magnetic stirring and, after a homogeneous mixture was obtained, the MWCNT/TX-100/IPA solution was slowly added to the PDMS/IPA solution under stirring (Figure 1(3)). Then, the temperature was set to 80 $^{\circ}\text{C}$, to gradually evaporate the solvent, while maintaining the stirring at 400 rpm. To ensure the evaporation of the solvent, the composite was kept in a ventilated box oven at 80 $^{\circ}\text{C}$ overnight (Figure 1(4)). Afterward, the curing agent was added in the proportion of 1:10 (Figure 1(5)), and the composite was spread over a PET film with the aid of a thin-film applicator (Gardco) set to a thickness of 400 μm . As the MWCNT infill is increased, the polymer paste becomes increasingly viscous. Thus, for infill percentages above 5.5 wt%, the polymer becomes too pasty and it was not possible to blade coat it with homogeneous thickness. Nevertheless, the samples with 8.0 and 10.0 wt% were obtained using a rolling pin.

The width of all the samples was controlled using masking tape (Figure 1(6)). Finally, the composites were cured at 120 $^{\circ}\text{C}$ for 30 min. In the samples where SB was added, the temperature prompted the SB to react thermally, releasing evaporated water, and CO_2 , which acted as the foaming agent of the composite, leading to the formation of pores within the MWCNT/PDMS matrix.

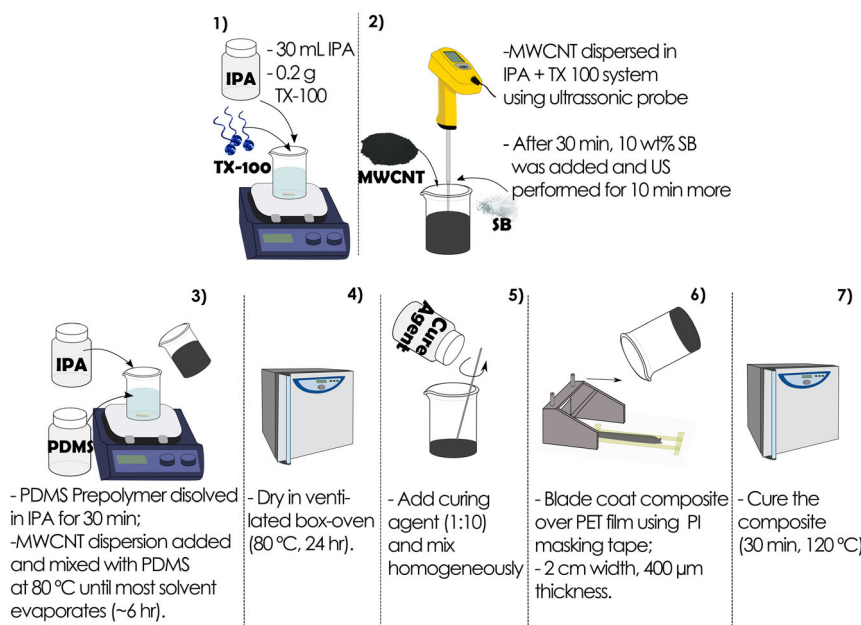


Figure 1. MWCNT/PDMS composite manufacturing steps and used equipment. SB was added to develop the porous composites. The 7 steps described in the figure include 1) mixing IPA with surfactant, 2) homogenizing with ultrasonic probe and adding SB, 3) dissolving PDMS precursor in IPA and adding homogenized MWCNT, 4) drying the IPA at ventilated box-oven, 5) adding curing agent, 6) blade coating the resulting material, and 7) curing the composite.

2.2.2. Electrical Properties of the Composites

The electrical properties of the prepared bulk composite were measured using an Ecopia Hall Effect Measurement System (HMS-5300). This equipment allowed the acquisition of electrical conductivity data from the prepared composites through a four-point probe setup. Before testing, the samples were cut in the shape of 1.0 cm by 1.0 cm squares. Conductivity was only measurable for samples with weight percentages equal to, or higher than 1.0 wt% MWCNT in PDMS.

2.2.3. Composite Characterization

The density of the porous and bulk MWCNT/PDMS composites was evaluated based on Archimedes' principle, resorting to a density kit (Mettler Toledo) assembled on a precision balance. IPA ($\rho = 0.785 \text{ g cm}^{-3}$) was used as the auxiliary liquid, and the density of the composite was calculated according to

$$\rho_{\text{composite}} = \frac{A}{A - B}(\rho_0 - \rho_L) + \rho_L \quad (1)$$

where A is the weight of the sample in air, B is the weight of the sample in the auxiliary liquid, ρ_0 is the density of the auxiliary liquid, and ρ_L is the density of air (0.0012 g cm^{-3}).

Stereo and Optical Microscopy (Leica) were used to characterize the morphology of the samples and measure pore size and distribution. For this purpose, the Leica software, LAS X, was employed to treat the images and calculate the size of the pores for each sample. To prepare the samples for microscopy, thin sections were cut using a precision scalpel. Further analysis was conducted by scanning electron microscopy (SEM) (NanoSEM-FEI Nova 200). To analyze the side profile of the samples under SEM microscopy, they were sliced laterally using a cryogenic bath. All samples were then sputter coated with gold (Au).

Thermogravimetric (TGA) analysis was used to quantify the amount of MWCNT present in each sample, assuring the homogeneity of the dispersion and the integration of MWCNT in the desired percentages. The used equipment was TGA Q500 V6.7, from TA Instruments, and the experiments were conducted

under oxygen atmosphere. The heating rate was $10.00 \text{ }^\circ\text{C min}^{-1}$ from 40 to $800 \text{ }^\circ\text{C}$ under an oxygen flow of 60.0 mL min^{-1} . The TA Instruments analysis software was then used to quantify the mass loss percentage (%) and the mass change ($\% \text{ }^\circ\text{C}^{-1}$) that occurred throughout each one of the experiments.

To assess the interaction between the MWCNT and the PDMS, Fourier transform infrared (FTIR) spectroscopy (JASCO) was carried out in the range of $600\text{--}4000 \text{ cm}^{-1}$, using attenuated total reflection.

2.2.4. Mechanical Properties of the Composites

The mechanical properties of the composites with increasingly added MWCNT infill (2.0 wt% to 5.5 wt%) were measured using an Instron Universal Testing machine. The tests were carried out at room temperature, using a velocity of 50 mm min^{-1} and a grip distance of 47 mm. The tested samples were cut in a dog-bone shape from the previously prepared $400 \text{ }\mu\text{m}$ thickness films according to the DIN 53504-2017-03 standard for testing rubber materials. The dog-bone shape was reproduced from the work of Riehele et al. and is depicted in Figure S1, Supporting Information.^[45] For each sample type, eight test specimens were produced and evaluated. The assessed mechanical properties were the Young modulus, Secant modulus at 40% elongation, maximum strain, and maximum stress.

2.2.5. Electromechanical Properties of the Composites

The piezoresistive sensor units were produced according to Figure 2a, and their electromechanical response was studied using the setup presented in Figure 2b. The Tabletop TTA from IAI was controlled using preprogrammed sequences of movements developed on the PC Interface Software from XSEL. The movement sequences were defined along the z-axis and, at each step, the displacement on the z-axis was increased, amplifying the pressure sustained by the sensor, which was placed below the force gauge for simultaneously quantifying the forces applied to the sensor.

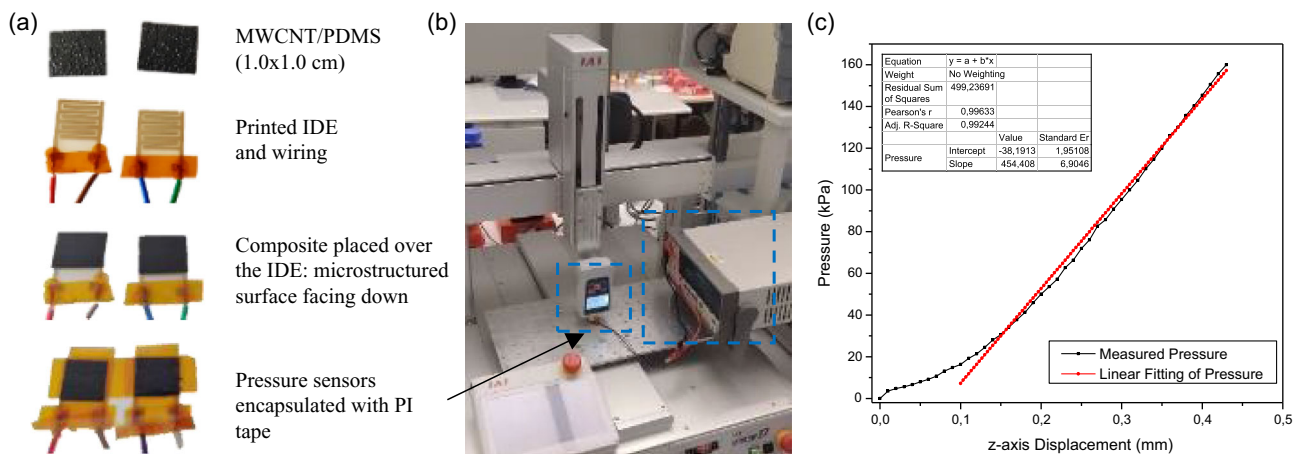


Figure 2. a) Pressure sensor unit assembly. b) Setup comprising the Tabletop moving table and arm coupled with the digital force gauge and multimeter. c) Calibration curve established between the z-axis displacement of the robotic arm and pressure sensed at the force gauge.

A calibration curve was extracted to correlate the displacement with the pressure sustained by the force gauge. As depicted in Figure 2c, a linear relationship was found between displacement and pressure from 0.1 mm.

Three different types of tests were performed on the samples. In the first one, continuously increasing pressure was applied, by lowering the tip of the force gauge 0.01 mm at each step. Resistance data from the samples were recovered for a total displacement of 0.43 mm, which corresponded to a pressure variation from 3 to 160 kPa. To evaluate the reproducibility of the manufacturing process and measurement system, two different batches were prepared and data from four sensors (two from each batch) were studied. The second test measured the electrical behavior of the samples when subjected to a stepwise pressure increment, by applying on/off pressure. In both cases, the data were continuously registered by connecting the sensors to an Arduino, interfaced with a 16 bit ADC (ADS1115), which increased the resolution of recovered data. The sensors were connected to the Arduino using a voltage divider circuit with an equivalent resistor of 33 k Ω . The delay between each measurement was 50 ms and each on/off cycle lasted for a total of 1.25 s. Incremental pressure was applied from 3 to 160 kPa over a squared sensor of 1.0 \times 1.0 cm. The response and recovery times of the sensors were also evaluated. Finally, the stability of the sensors was evaluated throughout 500 cycles.

2.2.6. Case Studies

For proof of concept, a 4 \times 3 sensor array was screen printed resorting to a polyester screen printing board with a 71–48 Polyester White (PW) mesh number (71 cm⁻¹ mesh count, 48 μ m thread nominal diameter, 90 μ m mesh opening, 41% open area, and 75 μ m mesh thickness). The used screen printer was the manual Miniprint, the substrate was PET, and the silver paste (Dycotec, DM-SIP-30 655) was used to print the conductive tracks of the array design, as illustrated in Figure 3a. After printing, 12 1.0 cm by 1.0 cm squares of MWCNT/PDMS composite were cut and positioned over the sensor array. To better isolate each sensor unit, rectangles of pristine PDMS “pillars”, with the same thickness as the sensing composite were added around

each taxel. To conclude, the array was encapsulated and isolated using polyimide tape, as depicted in Figure 3b. The 12 sensor taxels were connected to an Arduino using a multiplexer with 16 data inputs, which interfaced the sensors through a voltage divider circuit. The analog to digital conversion was processed at the Arduino and the graphic interface that allowed for continuous tracking of voltage output data was developed on the open-source coding platform Processing 4.0. Different weights were used to test the sensor array and, depending on the value of the chosen equivalent resistor (R_{eq}), the gain at the voltage divider could be adjusted, customizing the output voltage and sensing range (Figure 3c).

In this experiment, weights of 5, 10, 20, 100, and 250 g were used as well as two larger objects of 700 g and 2.250 kg. An equivalent resistor, of 10 k Ω , was used to study the range of the response of the pressure array. Another case study included in this work consisted of using a pressure sensor unit as a heart-beat sensor. To achieve this, the sensor was attached to a tight necklace and placed over the carotid artery. The sensor was connected to the Arduino through a voltage divider with an R_{eq} of 33 k Ω and the data were acquired at a rate of 50 ms.

3. Results and Discussion

3.1. Percolation Regime

To uncover the percolation threshold of the MWCNT/PDMS composites, their electrical performance was measured against the increasing weight percentage of MWCNT infill. The chosen concentrations were 0.1, 0.3, 0.5, 1.0, 2.0, 3.0, 5.5, 8.0, and 10.0 wt%. Figure S2, Supporting Information, depicts the variation in visual appearance of the MWCNT/PDMS pastes as the MWCNT concentration becomes higher. In this study, only bulk samples were evaluated. After curing, the electrical conductivity of each one of the composites was measured using the 4-point-probe method. This allowed for the establishment of a relationship between conductivity and MWCNT infill, providing the percolation threshold estimation. The results are presented in Figure 4a, alongside a graphical representation of nonconductive and conductive pathways. Samples with infill lower than

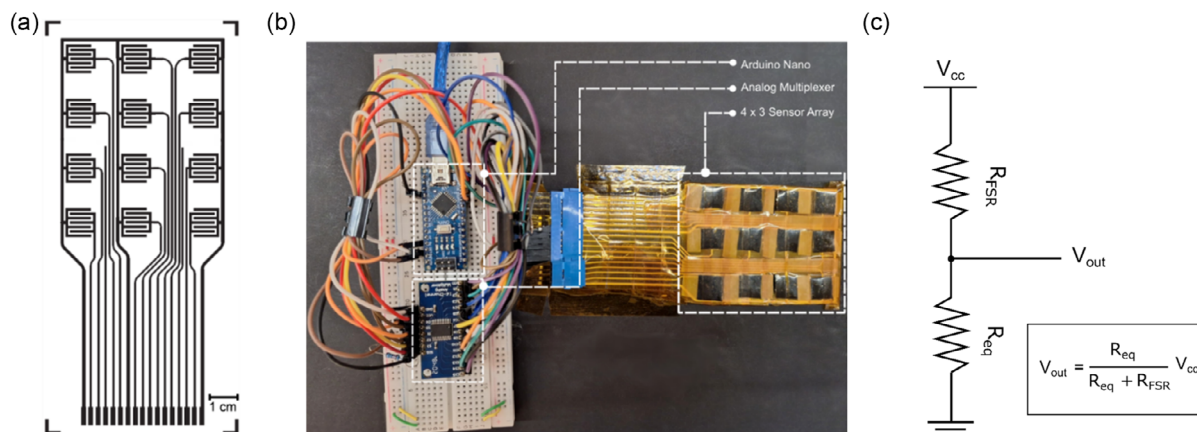


Figure 3. a) Sensor array design, as developed for the screen printing board. b) Sensor array and connections to the multiplexer and Arduino on the breadboard. c) Voltage divider circuit and measured voltage (V_{out}) equation. V_{cc} is the input voltage and R_{FSR} represents the force sensor resistor.

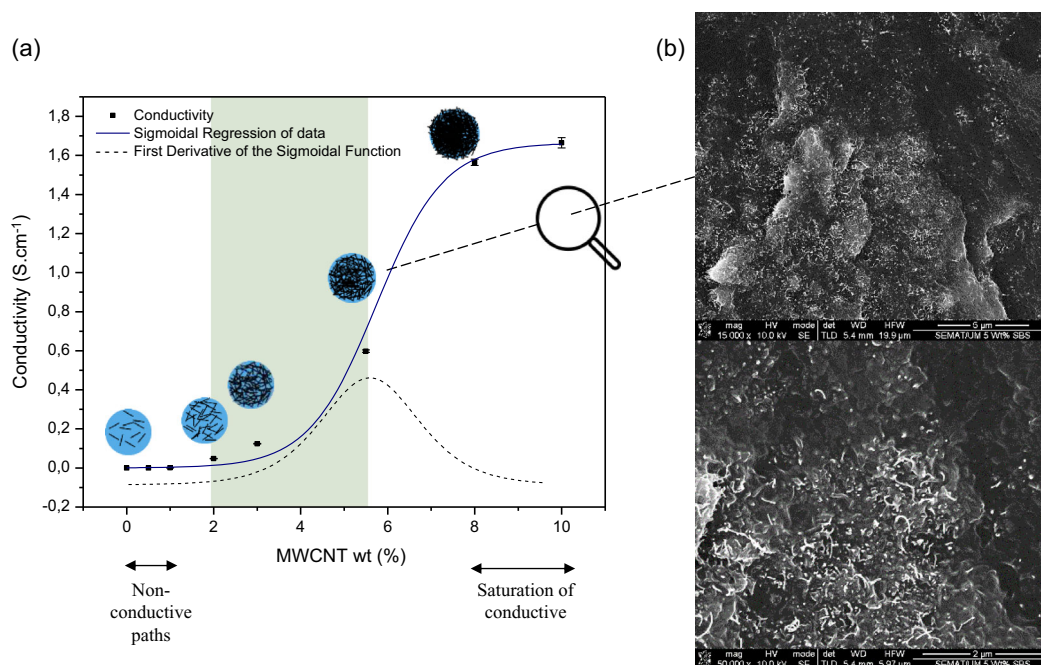


Figure 4. a) Conductivity of the MWCNT/PDMS composites with increasing MWCNT infill (■), sigmoidal regression fitting of the data (—), and first derivative of the fitted data (---). The data are illustrated with a graphical representation of the establishment and saturation of the conductive paths and the area where the electrical conductivity variation starts to increase until it peaks are highlighted in a darker rectangle. b) SEM images of the composites with 5.5 wt% infill, exhibiting proper dispersion of the MWCNT (15 000× and 50 000× magnifications).

1.0 wt% in MWCNT were not conductive. The experimental data were fitted using a sigmoidal regression.^[46,47] By calculating the first derivative of the sigmoidal function, the result is a Gaussian function that peaks at the inflection point of the sigmoid. This peak corresponds to the MWCNT concentration that results in the highest conductivity increase, which, as depicted in Figure 4a, occurs near the 5.5 wt% MWCNT infill concentration. The area where the conductivity variation increases is highlighted in the image and encompasses 2.0, 3.0, and 5.5 wt% infill concentrations. In Figure 4b, SEM images of the sample with 5.5 wt% in MWCNT are presented. These images portray a proper dispersion of MWCNT in the examined area (magnification: 15 000×).

3.2. MWCNT/PDMS Composites Characterization

3.2.1. Density

The density of the MWCNT/PDMS composites was evaluated through the Archimedes' principle. Significant density differences were registered between the bulk and porous composites. According to the results presented in Table 1, the density of the bulk samples falls within the typical density values of PDMS, which ranges between 0.96 and 1.05 g cm⁻³.^[48,49] Adding MWCNT to PDMS reduces the density of the composites due to the lower density of MWCNT. Moreover, the porous samples presented lower density than their bulk counterparts, with the 3.0 wt% MWCNT/PDMS sample presenting the lowest density (0.887 ± 0.008 g cm⁻³) and the 5.5 wt% MWCNT/PDMS sample presenting the highest density (0.995 ± 0.018 g cm⁻³).

Table 1. Summary of the density and pore volume estimation obtained for different samples and pore volume ratio estimation for each one of the porous samples, taking into account their respective bulk density.

	MWCNT infill [%]	Measured density	Standard deviation	Pore volume ratio estimation [%]
Bulk samples	0.0	1.026	0.010	—
	1.0	1.002	0.009	
	2.0	1.003	0.022	
	3.0	1.001	0.003	
	5.5	1.007	0.009	
Porous samples	2.0	0.948	0.007	5.4
	3.0	0.887	0.008	11.3
	5.5	0.995	0.018	1.2

This difference in material density correlates with the fact that the samples with 3.0 wt% infill developed larger pores than the other samples, whereas the samples with 5.5 wt% infill displayed fewer and underdeveloped pores.

As presented in Table 1, adding the foaming agent to the 2.0 wt% MWCNT/PDMS composite reduces its density by 5.4%, as compared with the bulk samples. For the 3.0 wt% MWCNT/PDMS composite, this reduction increases, reaching 11.4%. However, for the 5.5 wt% MWCNT/PDMS composite, the density reduction is merely 1.2%. This suggests a high interaction between the material viscosity and the foaming process (porous nucleation and growth). As the viscosity of the

composites with 5.5 wt% in MWCNT was higher, the tension forces at the polymer matrix limited the nucleation and growth size of the foaming agent. Table 1 summarizes the density values measured in this experiment and the pore volume ratio estimation.

3.2.2. Microscopy

To measure the average pore diameter, the composite was cross-sectioned and subsequently analyzed at the magnifying glass and microscope, using the image software of the microscope (Leica Application Suite microscope). The porous samples have an average pore diameter of $0.035 \pm 0.016 \text{ mm}^2$, $0.040 \pm 0.023 \text{ mm}^2$, and $0.012 \pm 0.006 \text{ mm}^2$ for 2.0 wt% MWCNT, 3.0 wt% MWCNT, and 5.5 wt% MWCNT, respectively. When no SB was added to the formulation of the composite, no pores were formed. The results of the microscope analysis of the samples' sectional porosity are summarized in Table 2.

By analyzing the porous samples, we could also identify domes on the surface of the composites, which have a prevalence of 65–71% in the samples with 3.0 and 2.0 wt%, respectively, whereas the surface of the other samples did not present domes. The domes that appeared in the material during the foaming process are a consequence of the liberation of the CO_2 , which not only led to the development of the pores but also pushed the surface of the composite directly above the pores. In the particular case of the samples with 5.5 wt% in MWCNT, the size of formed

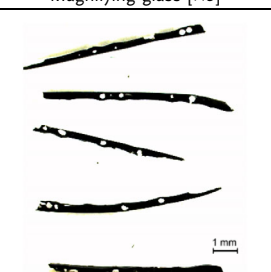
pores and superficial microstructure were considerably smaller than the ones registered for the other samples. This is correlated with the fact that the composite with 5.5 wt% in MWCNT exhibited higher viscosity precuring, limiting its ability to deform and develop microstructure during the foaming and curing step.

SEM images were also collected from the composites by cross-sectioning them using liquid nitrogen. As presented in Figure 5, some of the tendencies reported previously were also visible at $250\times$ magnification. Pores were larger for the 3.0 wt% composite, followed by the 2.0 wt% composite. Regarding the 5.5 wt% composite, the pores were visibly smaller and coalesced within themselves. As expected, for the bulk samples there were no noticeable pores, except for some gaps that were present in the 5.5 wt% bulk samples. Due to the increasingly viscous nature of these samples, air may have been entrapped inside the composite during the blade coating and curing of these samples. Moreover, in the images with $15\,000\times$ and $50\,000\times$ magnification, it can be highlighted that the dispersion of MWCNT during the formulation steps was successful for every concentration, as no MWCNT agglomerates were visible.

3.2.3. TGA and FTIR Analyses

TGA and FTIR analyses were performed on the six sets of samples (2.0, 3.0, 5.5 wt% MWCNT/PDMS bulk and porous composites). TGA was used to compare their thermal behavior as well as to assess the percentage of material that could be correlated with

Table 2. Summary of the morphologic analysis carried out with the magnifying glass and optical microscopy.

MWCNT [wt%]	Magnifying glass [$\times 3$]	Optical microscopy [$\times 6$]	Average pore section area [mm^2]	Proportion pore section/bulk area [%]
2.0			0.035 ± 0.016	11.23
3.0			0.040 ± 0.023	18.57
5.5			0.012 ± 0.006	4.21

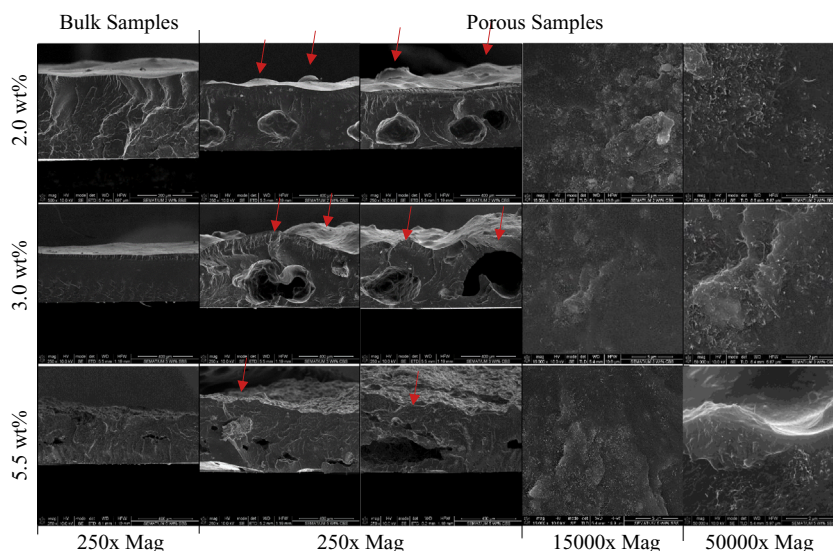


Figure 5. SEM images of the piezoresistive composites. Red arrows indicate the superficial bumps that occur as a consequence of the foaming process.

the MWCNT content in each one of those samples. In **Figure 6**, the weight loss curves of all the tested samples are presented. Pure PDMS is used as a reference in this study. The TGA experiments were carried out under oxygen atmosphere that allowed to identify the degradation interval of the MWCNT in the range of 600–700 °C, as depicted in **Figure 6c–h**.^[50–52] Concerning the thermal oxidative degradation of pure PDMS (**Figure 6b**, black line), three degradation peaks could be identified at around 308, 420, and 465 °C. Pure PDMS is thermally stable until 250 °C, which corresponds to its initial decomposition temperature (T_{id}). Hence, when PDMS reaches higher temperatures, its physical and mechanical properties begin to deteriorate. Thus, from 415 to 435 °C, the material undergoes an abrupt weight loss (maximum decomposition rate), which is caused by its depolymerization, characterized by the breaking of Si–O bonds in the PDMS chain.^[53] Finally, for temperatures higher than 465 °C, the PDMS byproducts continue to react with oxygen, and silicon dioxide (SiO₂) is produced. At the end of the TGA analysis, PDMS appears transformed into a white amorphous silica powder (insert image in **Figure 6b**).

Regarding the MWCNT/PDMS composites, the thermal degradation also starts at around 250 °C and is followed by the most substantial weight loss between 400 and 500 °C. However, it is noteworthy that the addition of carbon-based fillers decreased the velocity and extent of the thermal degradation of all the composites. The third degradation peak was also delayed, and, depending on the infill characteristics of the composite, it peaked between 550 and 590 °C. These changes to the degradation profile of the PDMS hint that MWCNT could be used as a thermal reinforcement, as proposed by Norkhairunnisa et al.^[54] Finally, the last degradation zone, which occurred between 550 and 800 °C, correlates with the degradation of the MWCNT content, as presented in **Figure 6c–h**.^[52] It is clear that with higher MWCNT infill, there is also a higher mass percentage degrading in the range of 550–800 °C. Moreover, the degraded mass percentage is identical to the original composite infill percentage,

as shown in **Table 3**. This is yet another indication that the MWCNT was homogeneously distributed throughout the different composites, as the measured mass attributed from the TGA experiments to the degradation of the carbon-based allotropes is very close to the percentage of MWCNT that was effectively dispersed to produce the composites.

As for the FTIR analysis, differences between the pristine PDMS and the MWCNT/PDMS composites were identifiable. Despite that, no significant differences were found between the bulk and porous composites. This suggests that even though SB is added during the formulation of the porous composites, their superficial chemical composition remains unaltered. As for the FTIR spectrums, depicted in **Figure 7**, characteristic transmission peaks and bands were present at 2965 cm⁻¹ (stretching of the C–H bond), 1260 cm⁻¹ (vibration of the Si–CH₃ bond), 1076 and 1015 cm⁻¹ (stretching vibration of the Si–O and Si–C bonds respectively), and 795 cm⁻¹ (plane bending vibration of the –CH₃ group). As represented in the inset image of **Figure 7**, it is visible that the characteristic peak at 2965 cm⁻¹ is reduced in transmittance percentage as the MWCNT infill increases. This correlates with an increase in the occurrence of C–H bonds, which result from the interactions between the MWCNT and the PDMS molecular chain.

3.3. Mechanical Properties of the MWCNT/PDMS Composites

The mechanical properties of the MWCNT/PDMS composites were also tested for the increasing MWCNT infill, for bulk and porous samples. The results of their stress–strain curves are presented in **Figure 8a**. All bulk samples exhibited superior mechanical behavior (stress and strain levels) than porous samples. It is worth mentioning that the shown engineering stress values are calculated based on the specimen cross-sections, and, in the particular case of porous samples, the effective cross-section reduction, due to the void content, was not considered (apparent stress values). The results for the Secant modulus,

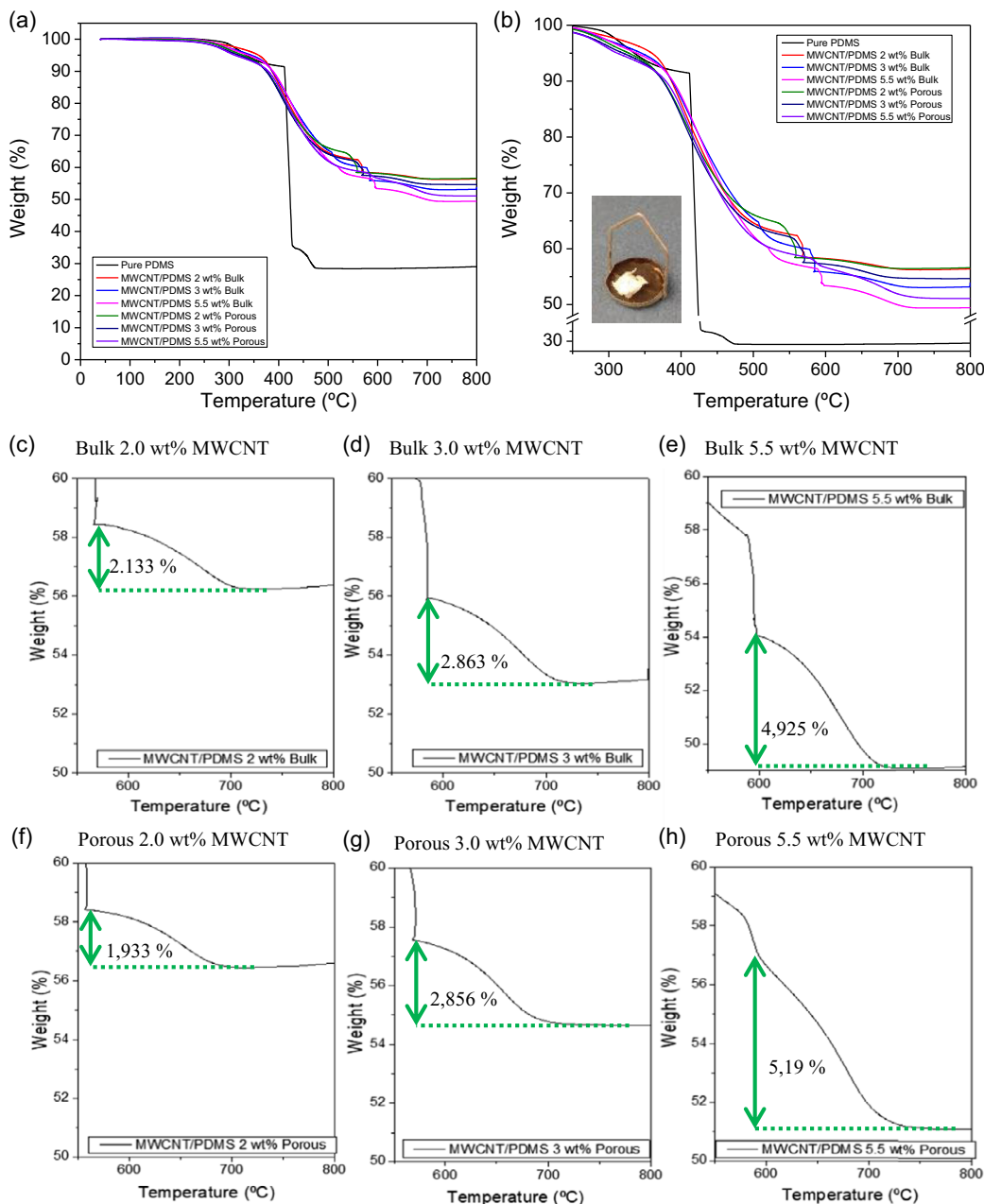


Figure 6. a) Thermal oxidative degradation curves of the MWCNT/PDMS samples. b) Collapsed view of the oxidative degradation thermal zone and indexed picture of the composite after the experiment. c–h) Close-up of the degradation curves at the MWCNT degradation zone (500–700 °C).

Table 3. Percentage of MWCNT infill in the composites as determined by TGA experiments.

		MWCNT infill [%]		
Expected, as per added during formulation		2.0	3.0	5.5
Experimental, as determined from TGA experiments (mass loss at the MWCNT degradation zone)	Bulk samples	2.1	2.9	4.9
	Porous samples	1.9	2.9	5.2

maximum stress, and maximum strain are presented in Figure 8b–e. According to the revision work of Ariati et al. pristine PDMS usually presents Young modulus between 1.32 and 2.97 MPa and maximum tensile strength verging from 3.51 to 5.13 MPa.^[55]

As depicted in Figure 8b, the Young modulus increases with MWCNT infill, due to the reinforcing nature of MWCNT. A similar tendency is registered for the Secant modulus, calculated for 40% of elongation (Figure 8c), which is, nevertheless, lower than

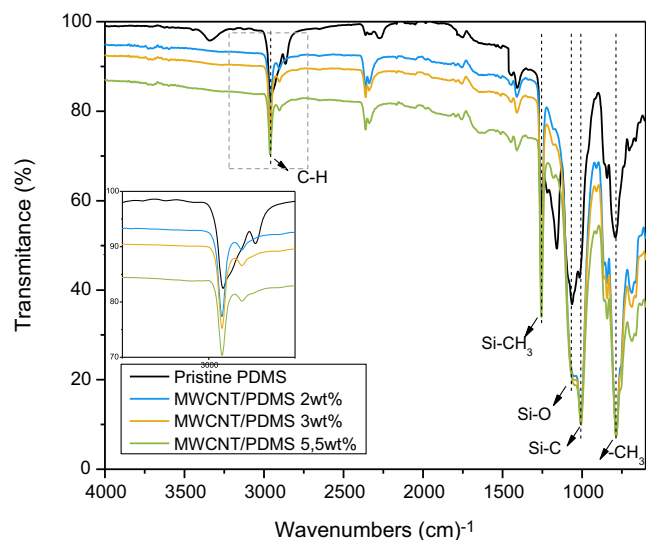


Figure 7. FTIR transmittance spectrums of pristine PDMS and MWCNT/PDMS composites with insert image of the C–H transmittance peaks.

the Young modulus values. As expected, for both cases, porous samples with 2.0 and 3.0 wt% of MWCNT present lower moduli than their bulk counterparts. This tendency is not present for the samples with 5.5 wt% in MWCNT that present similar moduli values for both porous and bulk samples. This may be due to the lower amount of void contents presented by the higher percentage MWCNT infill samples, as discussed previously. The maximum stresses (in this case also the ultimate tensile strength) of the composites are shown in Figure 8d. The maximum stress of the bulk composites presents values within the pristine PDMS boundaries until 3.0 wt% infill.

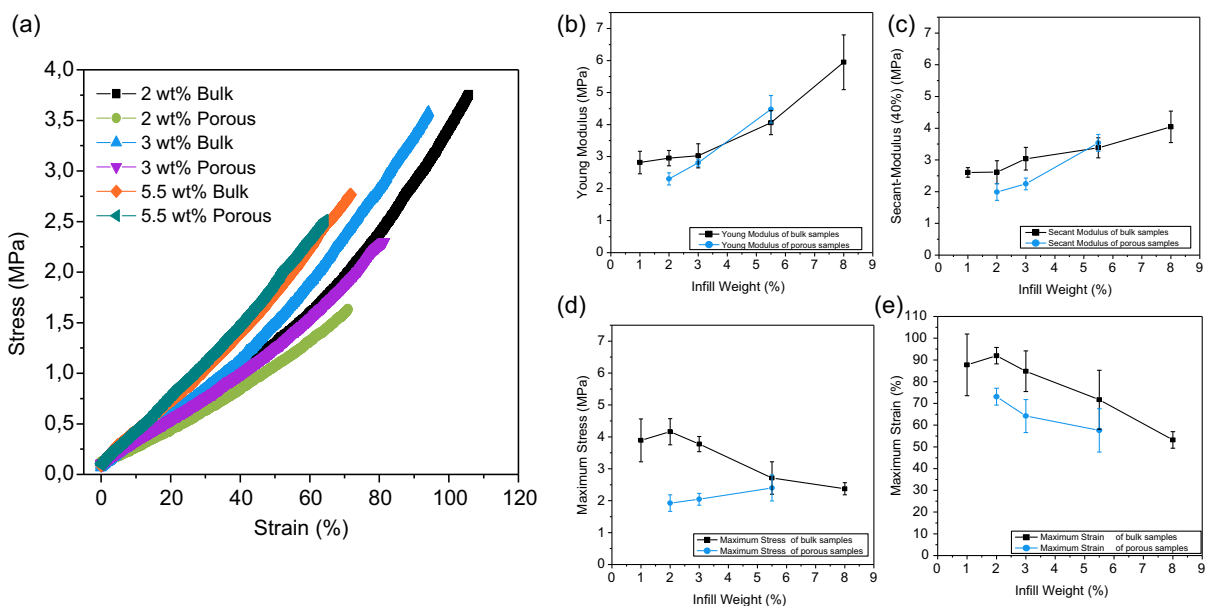


Figure 8. a) Stress–strain curves for MWCNT/PDMS bulk and porous composites ranging from 2 to 5.5 wt% of filler content. Mechanical properties of the MWCNT/PDMS composites against the infill percentage: b) Young modulus, c) Secant modulus at 40% of elongation, d) maximum stress, and e) maximum strain.

For infill of 5.5 wt% or higher, the maximum tensile stress sharply decreases, which means that for this MWCNT concentration, the mechanical properties of the bulk composite are deeply affected, possibly due to the presence of MWCNT agglomerates and their stress concentration effect. For the porous samples, the maximum stress is lower than the one of the bulk ones but slightly increases with MWCNT infill percentage, being higher at 5.5 wt% samples. Finally, the maximum strain sustained by the composite samples decreases with higher MWCNT infill, which means that samples with higher infill of MWCNT not only have lower tensile strain but also have lower ability to deform, failing at lower strain percentages (Figure 8e). The porous samples present a lower maximum strain than their bulk counterparts but present the same tendency that shows a decreasing maximum strain for samples with higher infill concentration. In summary, adding a higher percentage infill of MWCNT to the PDMS samples increases the Young and secant modulus of the composites but reduces the maximum stress and strain levels sustained. Creating a porous matrix reduces these values further.

3.4. Electromechanical Behavior of the Microstructured MWCNT/PDMS Composites

3.4.1. Electrical Properties at Rest

At first, the electrical properties of the composites with 2.0, 3.0, and 5.5 wt% in MWCNT were compared by measuring their electrical resistance at rest (without being forced under pressure). The composites were assembled over the printed IDE electrodes, as depicted in Figure 2a. The resulting values are summarized in Table 4 and, as expected, the initial electrical resistance of the samples decreases with increasing MWCNT infill. Moreover,

Table 4. Initial resistance (R_0) of each sample, measured when positioned at rest in contact with the IDE electrodes.

MWCNT [wt%]	R_0 bulk samples [Ω]	Variance [%]	R_0 porous samples [Ω]	Variance [%]
2.0	6.81×10^4	11.41	7.33×10^4	12.44
3.0	1.80×10^4	3.74	3.71×10^4	7.05
5.5	6.50×10^3	5.15	1.68×10^4	9.16

porous samples present a higher initial resistance than their bulk counterparts, which is consistent with the lower prevalence of conductive pathways in the porous samples at rest. Four sensors were tested for each concentration and porosity. The statistical variance was calculated for each set of sensors and it was found that sensors with a concentration of 2.0 wt% presented higher variance among them. This is probably related to the fact that they present a higher native resistance and are possibly below the percolation threshold. Variance was also higher for all the porous samples, which is a consequence of the development of the porous and bumpy structure within the sensors' matrix. Despite this, the calculated variance was <10% for the sensors with 3.0 and 5.5 wt% in MWCNT.

3.4.2. Electrical Properties Under Compressive Loading

To evaluate the electromechanical behavior of the samples, responses were collected and displayed in terms of electrical resistance (**Figure 9a,b**) and percentage of electrical resistance variation ($\Delta R/R_0$)% against increasing compressive loading (**Figure 9c,d**). Results obtained from two different batches (B1 and B2) are presented. Sensors from the two batches share the same tendencies and differences can be observed between bulk and porous samples and for different infill percentages, confirming that the addition of a porous structure within the matrix of the composite can be used to tune its electromechanical properties. From the results, it can also be concluded that the infill percentages of 3.0 wt% or 5.5 wt% in MWCNT are beneficial for the case of both bulk and porous samples and that the addition of porosity increased the sensitivity of all samples for lower pressure regimens. By using the data recovered in this test, the sensitivity of the samples was calculated by applying the following equation

$$\text{Sensitivity } (\% \text{ kPa}^{-1}) = \frac{\Delta R}{R_0} (\%) \times \frac{1}{\Delta P} \quad (2)$$

The electrical resistance variation–compressive load curves present a global nonlinear behavior, where three zones with different sensitivities can be identified, as illustrated in **Figure 9a,b**. The three sensitivity zones can be defined as follows.

Zone Sp_1 (0–10 kPa) corresponds to the initial part of the curve that shows a rapid, almost linear, variation of the electrical resistance with the compressive loading. This zone is dually affected by the infill concentration and the addition of a microstructure (pores and bumps). Sensitivity increases with infill concentration, especially from 2.0 to 3.0 wt% in MWCNT. Between the concentration of 3.0–5.5 wt%, the sensitivity increase is less pronounced, which might indicate the percolation threshold occurs

near these concentrations. Adding the microstructure further increased the sensitivity and resulted in a more controlled electrical resistance variation.

Zone Sp_2 (10–50 kPa) corresponds to the intermediate area of the curve that shows a steady variation but presents a more subtle slope in comparison with the slopes in Zone Sp_1 . This intermediate zone is clearly affected by the addition of porosity, which can be perceived across all the tested porous samples.

Zone Sp_3 (50–160 kPa) corresponds to the final part of the curve that is sensitive to higher loads. However, in this zone, the electrical resistance variation with pressure is smaller and tends to plateau. The sensitivity is greatly diminished in comparison with the previous zones and the effect of porosity is no longer perceivable.

The sensitivity was calculated for four sensors of each type and the results, and respective error, are exhibited in **Figure 9e**. In summary, all samples present the highest sensitivity in zone 1, varying between 6.18 and 8.00% kPa^{-1} . As discussed previously, the addition of porosity and microstructure improved the sensitivity for all samples. In contrast, increasing the concentration from 3.0 to 5.5 wt% in MWCNT did not increase the sensitivity significantly. In **Figure 9f**, a possible explanation of the sensing mechanism is depicted.

When the porous samples are at rest, their resistance is much higher than the resistance of their bulk counterparts, moreover, due to their bumpy surface, the contact area between the composite and the electrodes is decreased. When they are actuated by a low pressure, the pores and surface begin to suffer compression, which causes an enhanced resistance variation. This variation is smaller for bulk materials because their surface is in full contact with the electrodes, and therefore their initial resistance is much higher, resulting in a more abrupt establishment of electrically conductive pathways. In zone 2, the electrical-pressure sensitivities decrease, now varying in the range of 0.09–0.42% kPa^{-1} . In this zone, the highest sensitivity was similar for all the porous composites. Zone 3 presents the lowest sensitivity values, varying between 0.01 and 0.04% kPa^{-1} . In this zone, the values are similar for both bulk and porous composites, which behave alike. This indicates a complete compression of the pores in the porous samples, as illustrated in **Figure 9f**.

3.4.3. Electrical Properties Under Cyclic Compression

Another electromechanical test was performed, this time applying increasing pressure in a stepwise manner (loading/unloading pressure cycles). **Figure 10a–c** shows the variations in the electrical resistance values with repeated increase pressure/no pressure cycles from 3 kPa until 160 kPa. Each step lasted for 2.5 s. As expected, due to the compression of the conductive material, electrical resistance values decreased with incremental pressure. All the samples present a steady variation with pressure and can, therefore, be used as piezoresistive sensors in the range of at least 3–140 kPa; nevertheless, bulk samples with 3.0 and 5.5 wt% in MWCNT presented unstable readings for pressure higher than 150 kPa, suggesting saturation of the conductive pathways. As previously reported, the initial resistance of the porous samples is higher than the resistance of the bulk samples. This fact

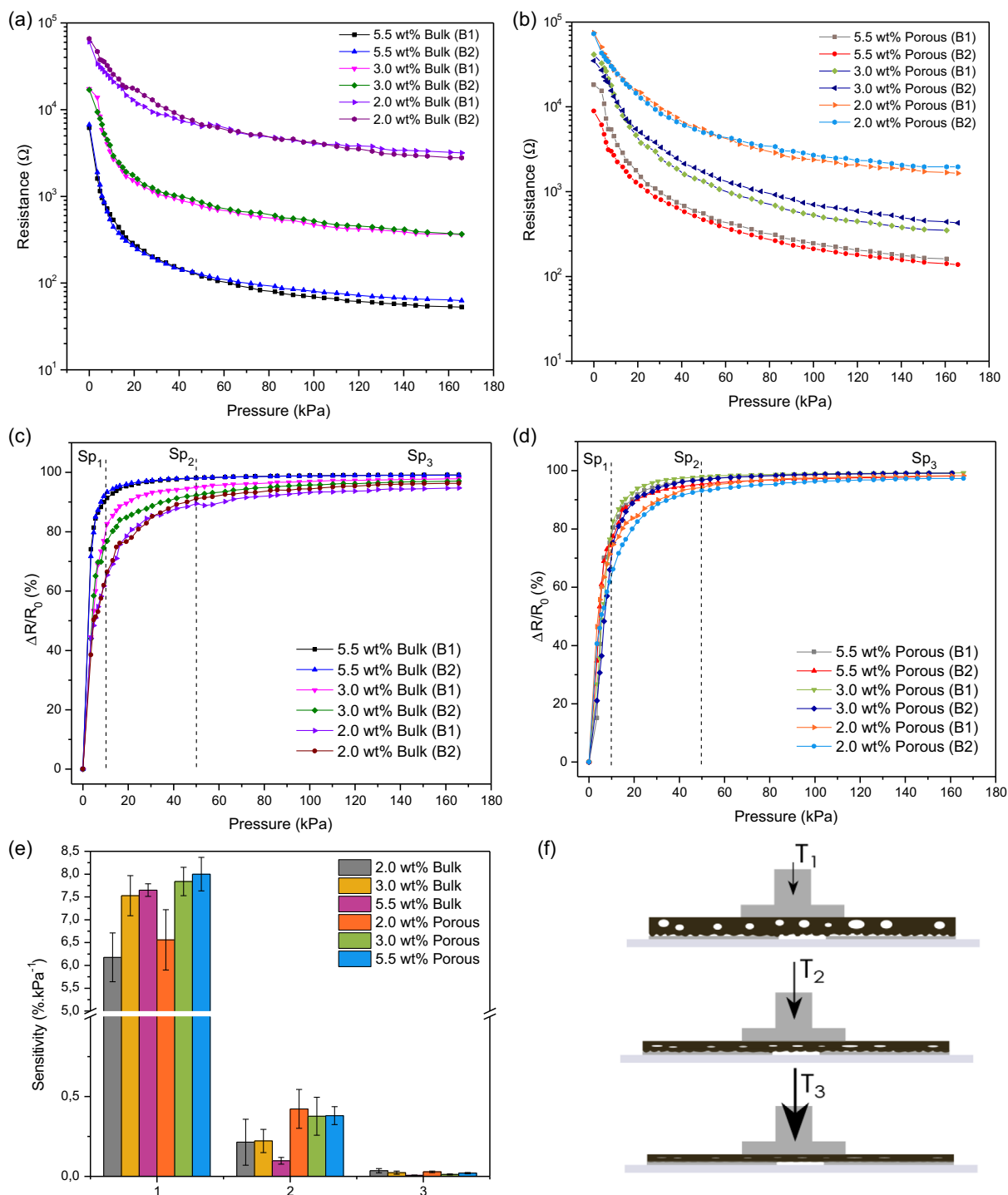


Figure 9. Electrical resistance response of the a) bulk and b) porous samples with increasing pressure (logarithmic scale). Percentual electrical resistance variation of c) bulk and d) porous samples with increasing pressure. Three different sensitivity zones (Sp) were determined and identified; e) sensitivity across the three zones and f) illustration of the sensing mechanism of the porous material.

contributes to a higher sensitivity to lower pressure for porous samples as the resistance variation is enhanced. For higher pressure, the resistance values of bulk and porous samples become increasingly closer, corroborating the results of the previous tests, as well as the proposed sensing mechanism. Taking into account

the electrical resistance variation range [37 100–300 Ω] and measured sensitivity obtained for the porous samples with 3.0 wt% in MWCNT, it was determined that this was the composite with the most interesting behavior to apply in further studies. Finally, to assess the repeatability of the sensor response, a long-term cyclic

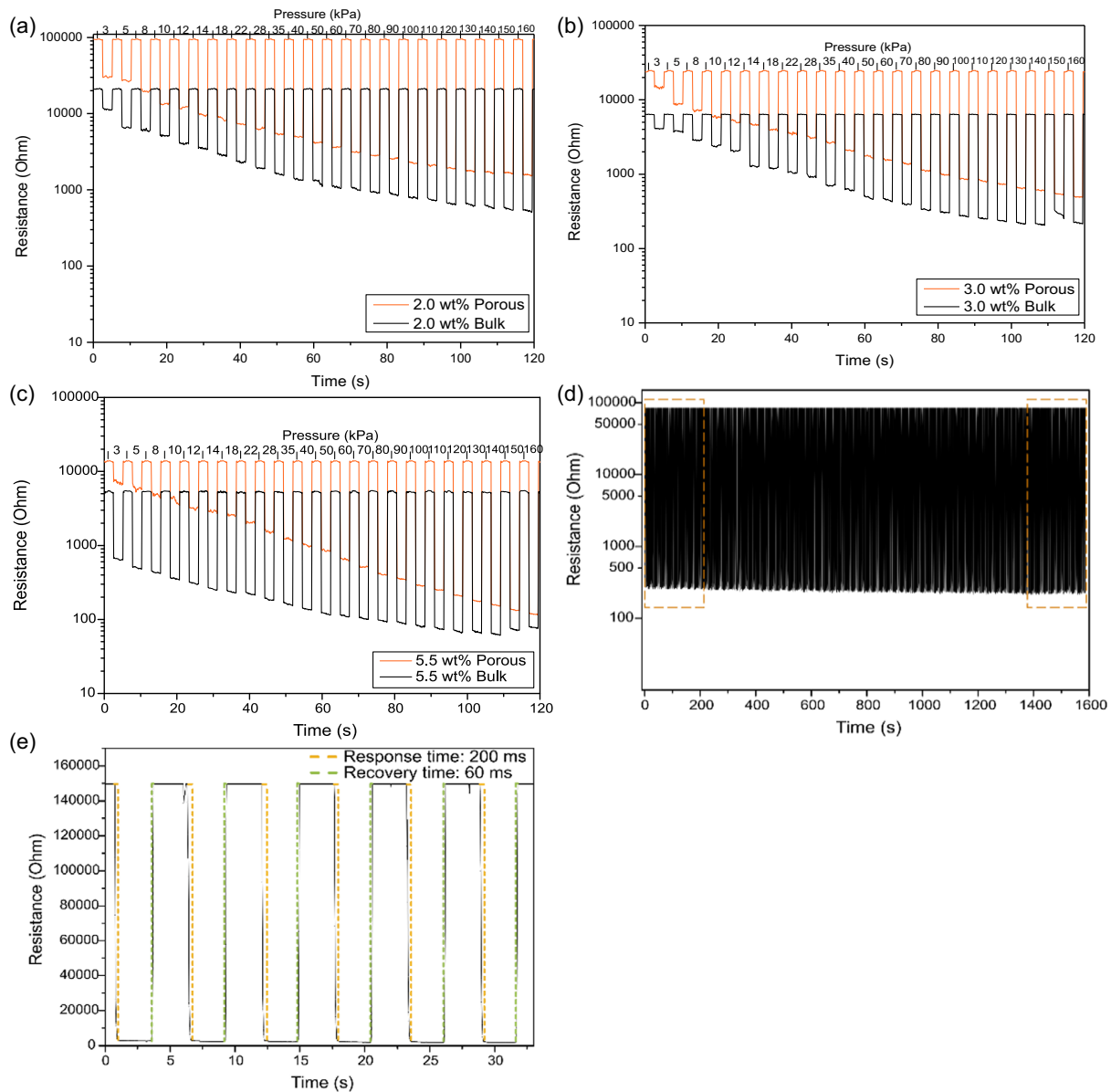


Figure 10. Stepwise increasing pressure experiment for a) samples with 2.0 wt% MWCNT infill, b) samples with 3.0 wt% MWCNT infill, c) samples with 5.5 wt% MWCNT infill, d) long-term cyclic pressure test (100 kPa on 3.0 wt% MWCNT porous sample), and e) response time of the sensors under study.

test was also performed by applying 500 cycles of on-and-off pressure of 100 kPa onto a porous sample with 3.0 wt% MWCNT infill. As presented in Figure 10d, the sample showed very good response and repeatability throughout the entire experiment, and almost no hysteresis occurred after 500 cycles. In addition, all samples demonstrated fast response and recovery times of 200 and 60 ms respectively, as presented in Figure 10e.

3.5. Case Studies

3.5.1. Pressure Sensing Array

To test the performance of the developed pressure sensors, squares of the 3.0 wt% MWCNT/PDMS porous composite were

assembled over a 3×4 screen-printed flat array. As described in Section 2.1, the data were acquired using an Arduino interfaced with a voltage divider, to further tune the sensitivity and sensing range of the sensors. The results acquired on the developed graphic user interface are presented as output voltage in Figure 11.

The data acquisition was aided by the use of a $10 \text{ k}\Omega$ equivalent resistor, which allowed for the detection and discrimination of weights from 5 to 2250 g. For all cases, the response and recovery times were very small ($\approx 200\text{--}60 \text{ ms}$) allowing for timely visualization of the results. As evidenced by the pictures in Figure 11, the developed composites were very thin, which allows the pressure-sensing array to be completely flat, flexible, and conformable. This type of device can be employed for the shape recognition of objects and human-machine interfacing.

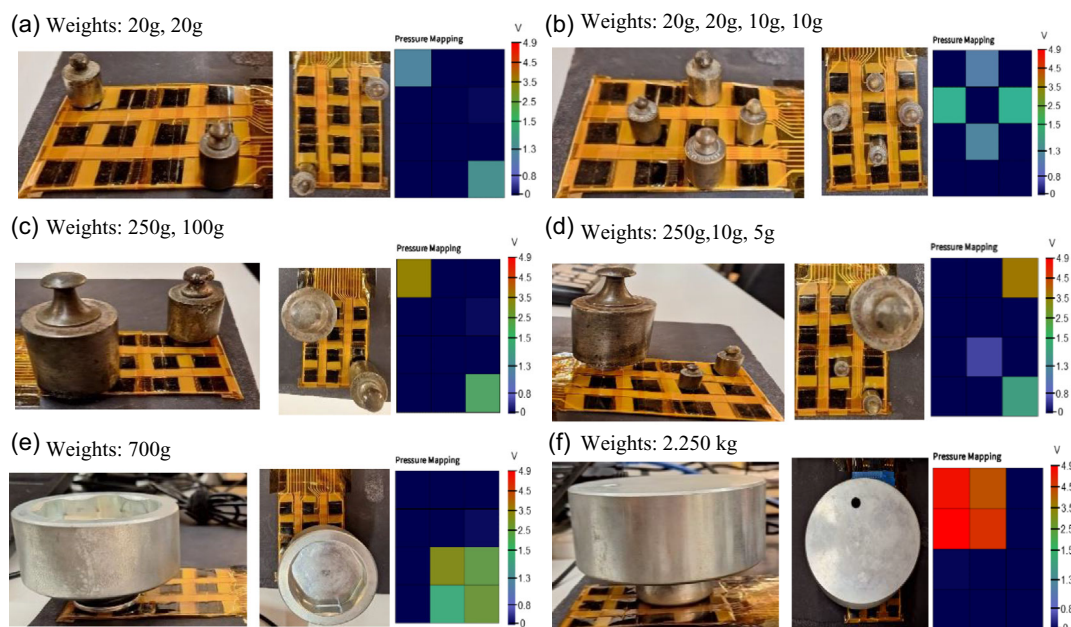


Figure 11. Exemplary images retrieved from the developed case study. a) Weights: 20, 20 g; b) Weights: 20, 20, 10, 10 g; c) Weights: 250, 100 g; d) Weights: 250, 10, 5 g; e) Weights: 700 g; f) Weights: 2.250 kg.

3.5.2. Heartbeat Monitor

The composite material was also applied for the development of a heartbeat monitor, as a way of proving its versatility. The sensor was placed over the right carotid artery of a test subject, and heartbeat data were gathered for a minute, as presented in **Figure 12**. Again, no electronic filtering or processing was applied to the gathered data, other than the use of a voltage divider. Nonetheless, the movement of the carotid artery was accurately detected in the form of resistance variation and the heartbeat rate could be easily calculated. In addition, the systolic pressure, diastolic pressure, and diastolic pressure peaks were distinguishable. These peaks constitute the normal arterial line waveform and can be used to estimate the arterial pressure.

4. Conclusions

In this work, porous and bulk MWCNT/PDMS composites were developed, using a simple dispersion technique, which avoided the use of hazardous solvents but granted a homogeneous distribution of MWCNT. The addition of MWCNT to PDMS, according to the filler concentrations reported for the percolation zone, allowed to obtain semiconductive composites with interesting piezoresistive behavior. Furthermore, it is believed that this work is the first to report the use of SB foaming to develop microstructure in the piezoresistive MWCNT/PDMS composites. Another advantage of the material herein developed is that the microstructure was generated within a thin film (400 μm), instead of a bulky sponge as frequently reported. This allows

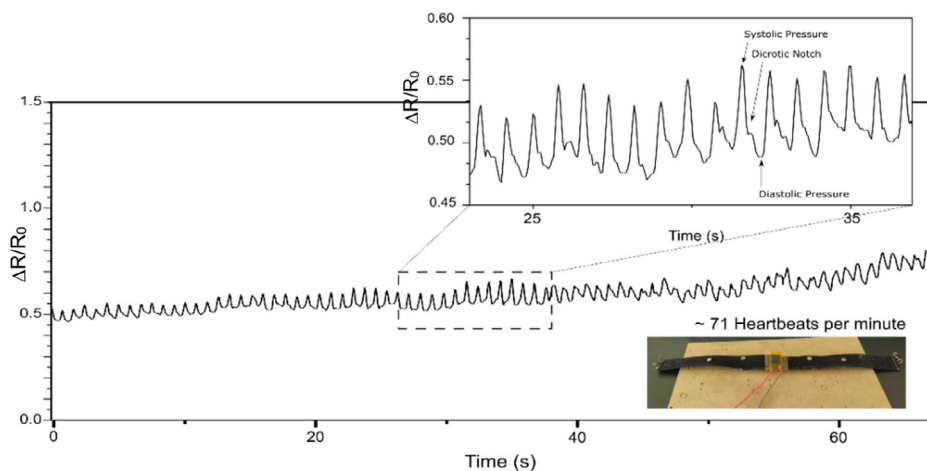


Figure 12. Schematic diagram of human heartbeat monitoring using the 3.0 wt% MWCNT/PDMS porous composite. Close-up plot of a section of data where the diastolic pressure, diastolic pressure, and dicrotic peaks can be identified.

for the integration of these sensors onto thin and flexible surfaces. Optical and SEM microscopy were used to study the porous matrix morphology in terms of pore size and density percentage, which was maximum for the 3.0 wt% MWCNT/PDMS porous composite, reporting a pore volume of 11.3%. Furthermore, as reported by the TGA experiments, the addition of MWCNT to the PDMS matrix improved the thermal characteristics of PDMS, delaying the degradation onset and reducing its extent. TGA was also used to corroborate the percentage of filler present in each one of the produced composites. Using FTIR analysis, the integration of MWCNT in the chemical structure of PDMS was confirmed as well. Regarding the mechanical characterization it was reported that higher percentage infill of MWCNT increased the Young and secant modulus of the composites, but they became more brittle. The creation of a porous matrix increased the plasticity of the materials but decreased their resistance to increasing strain.

Electromechanical tests provided further insight regarding the characteristics of the composites. Three sensing zones were determined and the highest sensitivity was reported for the initial sensing zone (<10 kPa). All porous composites presented very high sensitivity in this zone, which varied between 6.56 and 8.00% kPa⁻¹. From 10 to 50 kPa of applied pressure, the sensitivity was superior for the porous sensors as well, varying between 0.38 and 0.42% kPa⁻¹. From 50 to 160 kPa, sensitivity decreased to ≈0.04% kPa⁻¹. Good repeatability, low hysteresis, and appropriate response and recovery times were also proven for the composites. The characteristics of the sensors optimized in this work are presented comparatively to the ones reported in the literature in Table S1, Supporting Information. Finally, a proof-of-concept pressure sensor matrix and a heartbeat sensor were included, illustrating the resolution granted by the proposed piezoresistive porous composites.

To sum up, this work allowed to illustrate how the addition of microstructure to flexible pressure-sensing composites can be employed to enhance their sensitivity in low- and intermediate-pressure regimes. Moreover, a green and inexpensive manufacturing pathway was pursued, without any detriment to the dispersity of the MWCNT, nor to the chemical interaction between the MWCNT and the PDMS. A thorough evaluation of the material properties is presented granting that the characteristics of bulk and porous composites can be analyzed comparatively. Finally, the fact that sensitivity at least up to 160 kPa was reported for all the composites, places the performance of these sensors within the requirements defined in the literature for e-skins and biomonitoring applications.

Supporting Information

Supporting Information is available from the Wiley Online Library or from the author.

Acknowledgements

This work has been supported by NORTE-06-3559-FSE-000018, integrated in the invitation NORTE-59-2018-41, aiming the Hiring of Highly Qualified Human Resources, co-financed by the Regional Operational Programme of the North 2020, thematic area of Competitiveness and Employment, through the European Social Fund (ESF), and by the scope of projects

with references UIDB/05256/2020 and UIDP/05256/2020, financed by FCT—Fundação para a Ciência e Tecnologia, Portugal.

Conflict of Interest

The authors declare no conflict of interest.

Data Availability Statement

The data that support the findings of this study are available from the corresponding author upon reasonable request.

Keywords

flexible electronics, microstructured composite, piezoresistive sensors, pressure sensing composite, printed sensors

Received: January 26, 2024

Published online:

- [1] Y. Khan, A. Thielens, S. Muin, J. Ting, C. Baumbauer, A. C. Arias, *Adv. Mater.* **2020**, *32*, 1905279.
- [2] O. Kanoun, A. Bouhamed, R. Ramalingame, J. R. Bautista-Quijano, D. Rajendran, A. Al-Hamry, *Sensors* **2021**, *21*, 341.
- [3] Y. Guo, X. Wei, S. Gao, W. Yue, Y. Li, G. Shen, *Adv. Funct. Mater.* **2021**, *31*, 2104288.
- [4] C. S. Buga, J. C. Viana, *Flex. Print. Electron.* **2022**, *7*, 43001.
- [5] B. Nie, S. Liu, Q. Qu, Y. Zhang, M. Zhao, J. Liu, *Acta Biomater.* **2022**, *139*, 280.
- [6] Y. Zhang, T. Zhang, Z. Huang, J. Yang, *Adv. Sci.* **2022**, *9*, 2105084.
- [7] J. Chen, Y. Zhu, X. Chang, D. Pan, G. Song, Z. Guo, N. Naik, *Adv. Funct. Mater.* **2021**, *31*, 2104686.
- [8] L.-Y. Ma, N. Soin, *IEEE Sens. J.* **2022**, *22*, 3844.
- [9] U. Pierre Claver, G. Zhao, *Adv. Eng. Mater.* **2021**, *23*, 2001187.
- [10] J. C. Yang, J.-O. Kim, J. Oh, S. Y. Kwon, J. Y. Sim, D. W. Kim, H. B. Choi, S. Park, *ACS Appl. Mater. Interfaces* **2019**, *11*, 19472.
- [11] S. Kim, M. Amjadi, T.-I. Lee, Y. Jeong, D. Kwon, M. S. Kim, K. Kim, T.-S. Kim, Y. S. Oh, I. Park, *ACS Appl. Mater. Interfaces* **2019**, *11*, 23639.
- [12] M. R. Carneiro, M. Tavakoli, *IEEE Sens. J.* **2021**, *21*, 27374.
- [13] C. Ma, D. Xu, Y.-C. Huang, P. Wang, J. Huang, J. Zhou, W. Liu, S.-T. Li, Y. Huang, X. Duan, *ACS Nano* **2020**, *14*, 12866.
- [14] A. Ibrahim, M. Valle, *Electronic Skin: Sensors and Systems*, River Publisher, Gistrup, Denmark **2020**.
- [15] Z. Luo, X. Hu, X. Tian, C. Luo, H. Xu, Q. Li, Q. Li, J. Zhang, F. Qiao, X. Wu, V. Borisenko, J. Chu, *Sensors* **2019**, *19*, 1250.
- [16] W.-D. Li, K. Ke, J. Jia, J.-H. Pu, X. Zhao, R.-Y. Bao, Z.-Y. Liu, L. Bai, K. Zhang, M.-B. Yang, W. Yang, *Small* **2022**, *18*, 2103734.
- [17] X. Zhang, N. Li, G. Wang, C. Zhang, Y. Zhang, F. Zeng, H. Liu, G. Yi, Z. Wang, *RSC Adv.* **2023**, *13*, 16693.
- [18] Z. Han, Z. Cheng, Y. Chen, B. Li, Z. Liang, H. Li, Y. Ma, X. Feng, *Nanoscale* **2019**, *11*, 5942.
- [19] L. Wang, X. Huang, D. Wang, W. Zhang, S. Gao, J. Luo, Z. Guo, H. Xue, J. Gao, *Chem. Eng. J.* **2021**, *405*, 127025.
- [20] C. Yiu, T. H. Wong, Y. Liu, K. Yao, L. Zhao, D. Li, Z. Hai, H. Zheng, Z. Wang, X. Yu, *Coatings* **2020**, *10*, 711.
- [21] Y.-F. Wang, T. Sekine, Y. Takeda, J. Hong, A. Yoshida, D. Kumaki, T. Shiba, S. Tokito, *Adv. Mater. Technol.* **2021**, *6*, 2100731.
- [22] K.-C. Jung, J.-H. Son, S.-H. Chang, *Adv. Mater. Technol.* **2021**, *6*, 2000872.

- [23] Q. Xia, S. Wang, W. Zhai, C. Shao, L. Xu, D. Yan, N. Yang, K. Dai, C. Liu, C. Shen, *Compos. Commun.* **2021**, *26*, 100809.
- [24] S. Zhang, H. Liu, S. Yang, X. Shi, D. Zhang, C. Shan, L. Mi, C. Liu, C. Shen, Z. Guo, *ACS Appl. Mater. Interfaces* **2019**, *11*, 10922.
- [25] Y. Li, C. Zheng, S. Liu, L. Huang, T. Fang, J. X. Li, F. Xu, F. Li, *ACS Appl. Mater. Interfaces* **2020**, *12*, 23764.
- [26] K. Huang, H. Ning, N. Hu, F. Liu, X. Wu, S. Wang, Y. Liu, R. Zou, W. Yuan, Alamusi, L. Wu, *Compos. Sci. Technol.* **2020**, *192*, 108105.
- [27] J. O. Akindoyo, N. H. Ismail, M. Mariatti, *J. Mater. Sci. Mater. Electron.* **2021**, *32*, 12648.
- [28] D. Rajendran, R. Ramalingame, A. Adiraju, H. Nouri, O. Kanoun, *J. Compos. Sci.* **2022**, *6*, 26.
- [29] T. Gong, J. Jia, X.-R. Sun, W.-D. Li, K. Ke, R.-Y. Bao, W. Yang, *Carbon* **2023**, *206*, 53.
- [30] J. Hwang, Y. Kim, H. Yang, J. H. Oh, *Compos. Part B Eng.* **2021**, *211*, 108607.
- [31] B. Herren, V. Webster, E. Davidson, M. C. Saha, M. C. Altan, Y. Liu, *Nanomaterials* **2021**, *11*, 1740.
- [32] Z. Sang, K. Ke, I. Manas-Zloczower, *Small* **2019**, *15*, 1903487.
- [33] S.-W. Dai, Y.-L. Gu, L. Zhao, W. Zhang, C.-H. Gao, Y.-X. Wu, S.-C. Shen, C. Zhang, T.-T. Kong, Y.-T. Li, L.-X. Gong, G.-D. Zhang, L.-C. Tang, *Compos. Part B Eng.* **2021**, *225*, 109243.
- [34] W. Hao, J. Guo, C. Wang, S. Wang, C. Shi, *IEEE Access* **2020**, *8*, 142810.
- [35] E. Rostami-Tapeh-Esmaeil, A. Vahidifar, E. Esmizadeh, D. Rodrigue, *Polymers* **2021**, *13*, 1565.
- [36] C.-F. Cao, P.-H. Wang, J.-W. Zhang, K.-Y. Guo, Y. Li, Q.-Q. Xia, G.-D. Zhang, L. Zhao, H. Chen, L. Wang, J.-F. Gao, P. Song, L.-C. Tang, *Chem. Eng. J.* **2020**, *393*, 124724.
- [37] Y. Li, C.-F. Cao, S.-N. Li, N.-J. Huang, M. Mao, J.-W. Zhang, P.-H. Wang, K.-Y. Guo, L.-X. Gong, G.-D. Zhang, L. Zhao, L.-Z. Guan, Y.-J. Wan, L.-C. Tang, Y.-W. Mai, *J. Mater. Chem. A* **2019**, *7*, 27032.
- [38] X. Wei, X. Cao, Y. Wang, G. Zheng, K. Dai, C. Liu, C. Shen, *Compos. Sci. Technol.* **2017**, *149*, 166.
- [39] X. Wu, Y. Khan, J. Ting, J. Zhu, S. Ono, X. Zhang, S. Du, J. W. Evans, C. Lu, A. C. Arias, *Adv. Electron. Mater.* **2020**, *6*, 1901310.
- [40] Y. Zhang, Y. Zhao, W. Zhai, G. Zheng, Y. Ji, K. Dai, L. Mi, D. Zhang, C. Liu, C. Shen, *Chem. Eng. J.* **2021**, *407*, 127960.
- [41] W.-D. Li, J.-H. Pu, X. Zhao, J. Jia, K. Ke, R.-Y. Bao, Z.-Y. Liu, M.-B. Yang, W. Yang, *J. Mater. Chem. C* **2020**, *8*, 16774.
- [42] Z. Wang, X. Guan, H. Huang, H. Wang, W. Lin, Z. Peng, *Adv. Funct. Mater.* **2019**, *29*, 1807569.
- [43] S. Masihi, M. Panahi, D. Maddipatla, A. K. Bose, X. Zhang, A. J. Hanson, V. Palaniappan, B. B. Narakathu, B. J. Bazuin, M. Z. Atashbar, in *2019 IEEE Sensors*, **2019**, pp. 1–4.
- [44] M. Panahi, S. Masihi, D. Maddipatla, A. K. Bose, S. Hajian, A. J. Hanson, V. Palaniappan, B. B. Narakathu, B. J. Bazuin, M. Z. Atashbar, in *2020 IEEE Int. Conf. Flex. Printable Sensors Syst.*, **2020**, pp. 1–4.
- [45] N. Riehle, S. Thude, A. Kandelbauer, S. Thanos, G. Tovar, G. Lorenz, *JoVE* **2019**, *5*, 8590.
- [46] G. Arias-Ferreiro, A. Lasagabáster-Latorre, A. Ares-Pernas, M. S. Dopico-García, N. Pereira, P. Costa, S. Lanceros-Mendez, M.-J. Abad, *Adv. Electron. Mater.* **2022**, *8*, 2200590.
- [47] M. T. Tran, T. T. Tung, A. Sachan, D. Losic, M. Castro, J. F. Feller, *Carbon* **2020**, *168*, 564.
- [48] H. Cho, H. Moon, H. Lee, Y. T. Kim, S. Jeoung, *Bull. Korean Chem. Soc.* **2021**, *42*, 1225.
- [49] K. Izdihar, H. R. Abdul Razak, N. Supion, M. K. A. Karim, N. H. Osman, M. Norkhairunnisa, *Appl. Sci.* **2021**, *11*, 1172.
- [50] M. Protić, A. Miltojević, B. Zoraja, M. Raos, I. M. Krstić, *Teh. Vjesn. Gaz.* **2021**, *28*, 1762.
- [51] L. Malik, A. Pandit, A. Bashir, A. Qureshi, *J. Mater. Sci. Mater. Electron.* **2022**, *33*, 1.
- [52] D. Hu, H. Chen, Z. Yong, M. Chen, X. Zhang, Q. Li, Z. Fan, Z. Feng, *Mater. Sci. Appl.* **2013**, *04*, 453.
- [53] L. M. Al-Harbi, M. S. A. Darwish, M. M. Khowdiary, I. Stibor, *Polymers* **2018**, *10*, 507.
- [54] M. Norkhairunnisa, A. Azizan, M. Mariatti, H. Ismail, L. C. Sim, *J. Compos. Mater.* **2011**, *46*, 903.
- [55] R. Ariati, F. Sales, A. Souza, R. A. Lima, J. Ribeiro, *Polymers* **2021**, *13*, 4258.